Bull. Mater. Sci., Vol. 26, No. 4, June 2003, pp. 377–382. © Indian Academy of Sciences.

Preparation and characterization of Eu^{3+} activated $CaSiO_3$, $(CaA)SiO_3$ [A = Ba or Sr] phosphors

S J DHOBLE*, N S DHOBLE† and R B PODE‡

Kamla Nehru College, Sakkardara Square, Nagpur 440 009, India
†Sevadal Women's College, Sakkardara Square, Nagpur 440 009, India
‡Department of Physics, Nagpur University, Nagpur 440 010, India

MS received 27 December 1999; revised 4 March 2003

Abstract. **Eu^{3+} activated $CaSiO_3$, (Ca, Ba) SiO_3 and (Ca, Sr) SiO_3 have been prepared by sol–gel technique. Residual solvent and organic contents in the gel were removed by firing at 100°C for 3–4 h at 300 and 600°C for 2 h. Small exothermic shoulder around 850 to 875°C, as observed in DTA curve, corresponds to crystallization temperature of the doped calcium silicate. Influence of firing temperature on the luminescence of Eu^{3+} shows the maximum emission intensity in gel fired at 850°C. Photoluminescence emission peak is observed at 614 nm due to $^5D_0 \rightarrow {}^7F_2$ transition of Eu^{3+} ion in (Ca, Ba) SiO_3 and (Ca, Sr) SiO_3 phosphors, when excited by 254 nm. The (Ca, Ba) SiO_3 material is proposed as an efficient red phosphor.**

Keywords. **$CaSiO_3$; photoluminescence; sol–gel; phosphor.**

1. Introduction

Oxides, silicates, phosphates, borates and fluorides doped with rare earth ions have received great attention because of their potential applications in optical and laser devices. Koedam and Opstelten (1971) predicted a tri-colour lamp and development of lamp phosphors. Later on, Haft and Thornton (1972) developed the tri-colour lamp based on predictions. Theoretically it is predicted that good colour rendering index (CRI) can be obtained if three emission bands centred around 450 nm (blue), 540 nm (green) and 610 nm (red) are combined. Haft and Thornton used $Y_2O_3 : Eu^{3+}$ for red, Eu^{2+} doped strontium chlorapatite for blue and Mn doped zinc silicate for green emissions. Rare earth ions are known to exist in various valence states although the trivalent state is the most prevalent. Particularly Sm and Eu ions are known to be stable in trivalent as well as in divalent states. Photoluminescence (PL) of europium has been extensively studied in different hosts (Ohnishi 1983; Welker 1991; Upadeo and Moharil 1996; Otvos and Peto 1998; Band *et al* 1999). Eu^{3+} exhibits a red or orange luminescence, while Eu^{2+} strongly depends on the host and it may emit anywhere from UV to deep red region. Luminescence of Eu^{3+} has been used to obtain the red component of the full colour display devices (Raue *et al* 1984; Smets 1987; Leskela and Niinitso 1992). The Eu^{3+} activated oxides have been extensively investigated due to their applications as red lamp phosphors (Wanmaker *et al* 1966; Blasse 1970). Recently, we have published Eu^{3+} activated $CaWO_4$ (Pode and Dhoble 1997) and A–BaGd $(PO_4)_2$ (A = Li, Na or K) (Band *et al* 1999) as red phosphors. Eu^{2+} has been extensively used in obtaining the blue component of lamp phosphors (Smets 1987), colour TV (Welker 1991), X-ray imaging phosphors (Wanmaker and ter Vrugt 1967; Meijerink and Blasse 1989; Crawford and Bixner 1991; Moharil 1994), in lamps for photocopying (Wanmaker and ter Vrugt 1967) etc. In recent years, Mn activated Zn_2SiO_4 has been found to be suitable for many more applications such as thin film electroluminescent devices (Ouyang *et al* 1996), plasma display panels (Cich *et al* 1998; Sohn *et al* 2000), medical imaging detector for low voltage radiography as well as fluoroscopy (Kandarakis *et al* 1998; Cavouras *et al* 2000). Silicates doped with rare earth ions have received great attention because of their potential applications in optical and laser devices. $CaSiO_3$ has been used as a raw material of tile and pottery (Kurczyk and Wuhrer 1971), a filler to resin (Jain *et al* 1992). X_2–$Y_2SiO_5 : Tb^{3+}$ is one of the best green emitting cathodoluminescence phosphors (Peters 1969; Rabinovich *et al* 1987) and X_2–$Y_2SiO_5 : Ce^{3+}$ is a good blue phosphor (Gomes and Bril 1969a,b). In most of the studies solid state diffusion technique has been used for the synthesis. In recent years, novel methods such as polymer pyrolysis (Su *et al* 1996), hydrothermal (Lu *et al* 2001), spray pyrolysis (Lenggoro *et al* 2000), sol–gel (Lin *et al* 2000; Ahmadi *et al* 2000; Zhang *et al* 2001) techniques, etc has been successfully employed for synthesis of silicate based phosphor. This paper presents the preparation of Eu^{3+} activated calcium based silicate phosphors which is prepared by sol–gel technique and charac-

*Author for correspondence

terized by photoluminescence (PL), X-ray diffraction (XRD), differential thermal analysis (DTA) and scanning electron microscopy (SEM) techniques.

2. Experimental

Eu doped $CaSiO_3$, (Ca, Ba) SiO_3 and (Ca, Sr) SiO_3 powders were prepared by sol–gel technique. Analar grade powder $CaCO_3$, tetra ethyl orthosilicate $[Si(OC_2H_5)_4]$/ $CaCO_3$, $Si(OC_2H_5)_4$, $BaCO_3/CaCO_3$, $Si(OC_2H_5)_4$, $SrCO_3$ were taken as starting materials for the preparation of $CaSiO_3$, (Ca, Ba) SiO_3 and (Ca, Sr) SiO_3, respectively in required proportion. For the preparation of doped sample known amount of impurity Eu_2O_3 was added to starting materials. $CaCO_3$, $BaCO_3/CaCO_3$, $SrCO_3$ were first dissolved in dilute nitric acid. Later on ethanol and double distilled water in the proportion of 2 : 1, were added to the above transparent nitrate solution. Subsequently ethyl orthosilicate was added to this solution in small instalments and stirred well. Ca/(Ca, Ba)/(Ca, Sr) nitrated and ethyl orthosilicate are soluble in ethanol. Diluted ammonia was added to the above solution that neutralizes the excess nitrate and results in the formation of gel. The gel thus formed was dried in air atmosphere for about 3–4 h at 100°C, calcined at 300 and 600°C for 3 h and then quenched to room temperature and then crushed to fine powder for further work.

Formation of silicate was confirmed by studying XRD pattern. Differential thermal analysis (DTA) was used to find the crystallization temperature of silicates. The surface morphology was investigated using SEM analysis. Photoluminescence spectrum was recorded on Jobin Yvon Spectroflurometer at room temperature.

3. Results and discussion

3.1 *DTA measurement*

Figure 1 shows the differential thermal analysis (DTA) curve of Eu doped $CaSiO_3$ powder. The DTA endothermic peak between temperature 200 and 325°C is attributed to the elimination of residual solvents. The second endothermic peak between 325 and 600°C is due to elimination of the organic compounds. The small exothermic effect around 850–875°C on the DTA curve can be attributed to crystallization of the $CaSiO_3$. Annealing at lower temperature may result in the formation of Ca_2SiO_4. The optimum firing temperature for crystallization was around 850–875°C that was confirmed by DTA measurement. These results are consistent with the results reported by Fan *et al* (1996).

3.2 *XRD measurement*

X-ray diffraction (XRD) pattern of doped silicate gel fired at 850°C is shown in figure 2. The observed pattern matched with the standard data of the compound (JCPDS file no. 27-88). $CaSiO_3$ monoclinic phase is present in large abundance along with small trace of Ca_2SiO_4 as orthorhombic phase. The crystal field symmetry and hence the effect of field on the shifting of emission lines is strongly dependent on the relative contents of these two phases. The following experiments are performed to study this effect.

3.3 *SEM analysis*

Particle size of phosphor plays an important role in deciding the luminescence quality of the material. Uniform particle size distribution and fine particles (< 5 μm) are some of the requirements of good luminescent materials. Figure 3 shows the SEM microphotograph of (Ca, Ba) $SiO_3 : Eu^{3+}$ phosphor. Average particles of phosphor with less than 3 μm is a good sign of lamp phosphor for coating purpose. SEM photograph of (Ca, Sr) $SiO_3 : Eu^{3+}$ also shows similar results, except that some changes in particle size was observed, therefore are not shown here.

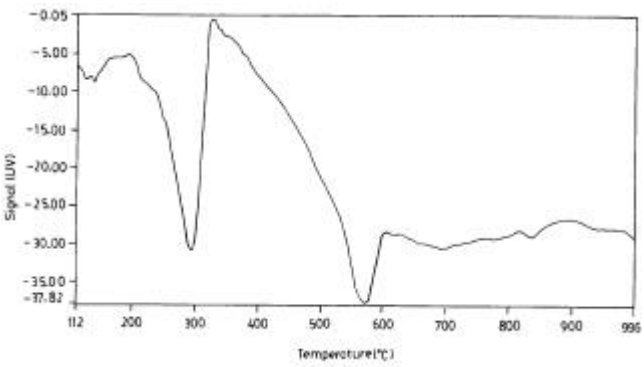

Figure 1. DTA curve for $CaSiO_3 : Eu^{3+}$ gel.

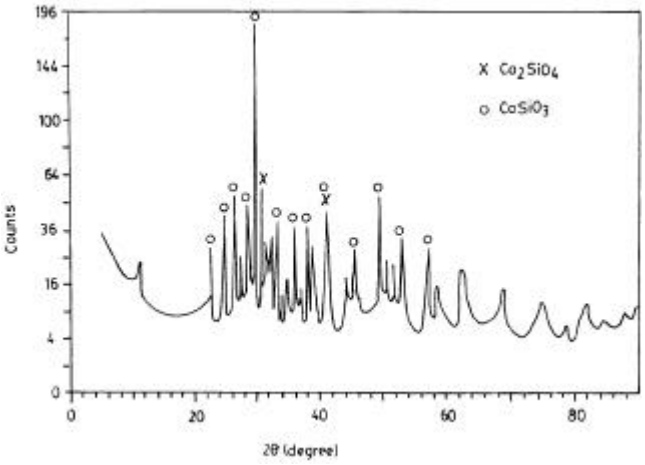

Figure 2. XRD pattern of $CaSiO_3 : Eu^{3+}$ gel fired at 850°C.

3.4 *PL measurements*

3.4a *PL in $CaSiO_3 : Eu$*: Figure 4 shows the influence of firing temperature on the luminescence of $CaSiO_3 : Eu^{3+}$ (3 mol%), excited at 399 nm. In a gel fired at 750°C, prominent peaks are at 594 and 618 nm besides a weak shoulder at 660 nm due to transitions: $^5D_0 \rightarrow {}^7F_1$, $^5D_0 \rightarrow {}^7F_2$ and $^5D_0 \rightarrow {}^7F_3$, respectively. The splitting of weak 618 line into two components was also observed. As the firing temperature is raised to 850°C, emission lines become strong. The 594 nm line due to $^5D_0 \rightarrow {}^7F_1$ is split into two components at 594 and 599 nm, whereas no appreciable splitting is observed for 618 nm line. The intensity of 618 nm line is three times more than 594 nm line. Further increase in firing temperature to 950°C, resulted in decrease in emission intensity of all lines due to the variation of interaction between Eu^{3+} and O^{2-} ions at higher temperature. The main band splits into three bands, 616, 620 and 622 nm, and the band corresponding to $^5D_0 \rightarrow {}^7F_1$ transition split into 590 and 597 nm. Due to strong interaction between Eu^{3+} and O^{2-} ions in fired gel, appreciable splitting of emission lines can be observed by the crystal field. The splitting of energy levels by crystal field is dependent on the symmetry of the field and relates to surroundings of Eu^{3+} ions in the crystal lattice. When Eu^{3+} ion is put into the Ca^{2+} site, which is coordinated by six O^{2-} ions, the splitting of energy levels by crystal field would change with the position of Eu^{3+} ion in the crystal lattice. Along with $CaSiO_3$, small amount of Ca_2SiO_4 phase is formed during firing experiments. The splitting of energy levels depends on the relative contents of $CaSiO_3$ and Ca_2SiO_4 in fired gel. In samples fired at 850°C, practically no splitting of 618 nm main peak was observed. It seems that relative concentration of $CaSiO_3$ phase is highest and Eu^{3+} may be surrounded by same environment in this sample. Eu^{3+} emission usually occurs from $^5D_0 \rightarrow {}^7F_j$ transitions. There are three transitions, which are of prime importance: $^5D_0 \rightarrow {}^7F_0$ (around 570 nm), $^5D_0 \rightarrow {}^7F_1$ (around 594 nm) and $^5D_0 \rightarrow {}^7F_2$ (around 610–630 nm). The first one is strongly forbidden transition and yet observed with appreciable intensity in some hold. The $^5D_0 \rightarrow {}^7F_1$ transition is allowed as magnetic dipole transition. This is the only transition when Eu^{3+} is situated at a site coinciding with a centre of symmetry. $^5D_0 \rightarrow {}^7F_2$ allowed as forced electric dipole transition and is induced when Eu^{3+} is situated at a site which lacks the inversion symmetry. This transition is much stronger than that of the transition to $^7F_1$ state. Further, all the lines corresponding to these transition split into number of components decided by the local symmetry.

Excitation spectrum of $CaSiO_3 : Eu^{3+}$ (3 mol%) shows two lines at 267 and 399 nm, monitored at 618 nm (results are not reproduced here). The emission spectra for 267 and 399 nm excitations are shown in figure 5. For 399 nm excitation two peaks are obtained around the wavelength 594 and 618 nm due to $^5D_0 \rightarrow {}^7F_1$ and $^5D_0 \rightarrow {}^7F_2$ transitions, respectively as described earlier (curve a). Small peak around 660 nm is also obtained due to $^5D_0 \rightarrow {}^7F_3$ transition. The intensity of 618 nm peak is almost three times more than 594 nm peak. When the sample is excited by 399 nm wavelength, Eu^{3+} ion is raised to $^5L_6$ level from ground state. During emission, Eu^{3+} ion decays stepwise from $^5L_6$ to $^5D_0$ level. Since the separation between $^5D_0$ and ^7F_j (where j = 0, 1, 2, 3, 4, 5 and 6) is large, the stepwise decay process stops here and returns to ground state by giving emission in the orange and red regions. If the impurity ion does not occupy centre of symmetry of the crystal lattice, then it will give both magnetic and electric dipole transitions (Oomen and van Dongen 1989). When the rare earth impurity ion is located at the centre of symmetry in the relevant crystal

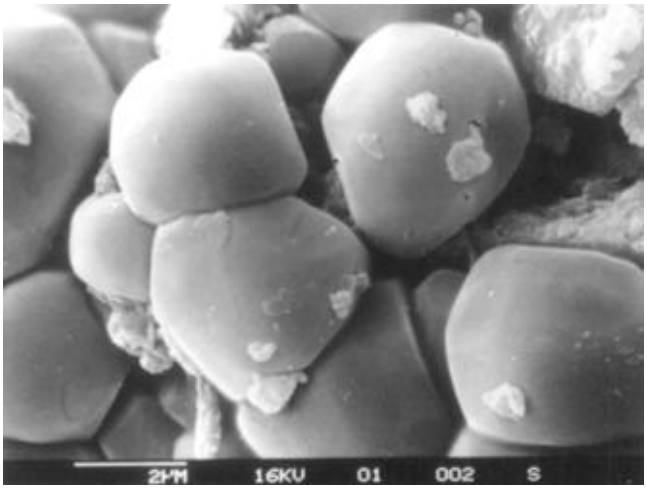

Figure 3. SEM microphotograph (× 10,000) of (Ca, Ba) $SiO_3 : Eu^{3+}$ phosphor.

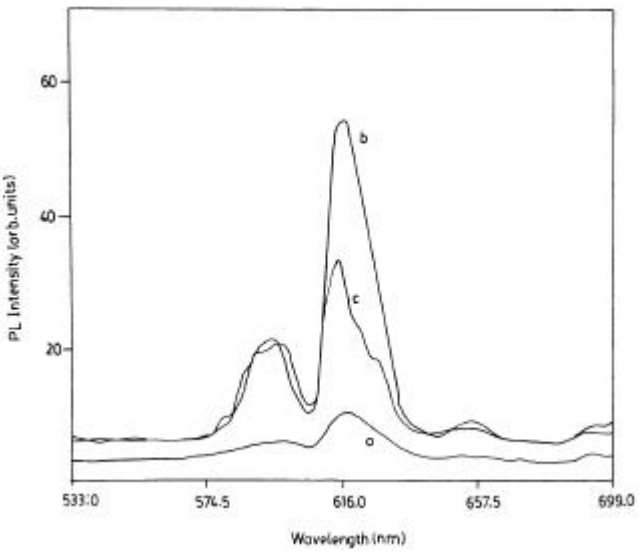

Figure 4. Photoluminescence emission spectra of the $CaSiO_3 : Eu^{3+}$ gel fired at a. 750°C, b. 850°C, and c. 950°C.

lattice, only magnetic dipole transitions are allowed. In the present case both magnetic and forced electric dipole transitions, $^5D_0 \rightarrow {}^7F_1$ and $^5D_0 \rightarrow {}^7F_2$ emission lines, respectively are observed. The forced electric dipole transitions arise from the lack of a centre of symmetry. The emission in the vicinity of 600 nm is due to the magnetic dipole transition $^5D_0 \rightarrow {}^7F_1$, which is insensitive to the site symmetry. The emission around 610–630 nm is due to the electric dipole transition of $^5D_0 \rightarrow {}^7F_2$, induced by the lack of inversion symmetry at the Eu^{3+} site, is much stronger than that of the transition to the $^7F_1$ state. Luminescence of Eu^{3+} ions in commercial red phosphors such as YVO_4, Y_2O_3 and Y_2O_2S, occupy the site that has no inversion of symmetry. The strong emission due to the electric dipole transition ($^5D_0 \rightarrow {}^7F_2$) in the materials is utilized for practical applications. If the Eu^{3+} site has inversion symmetry, as in Ba_2GdNbO_5, $NaLuO_2$ (Blasse and Bril 1970) and $InBO_3$ (Avella *et al* 1967), the electrical dipole emission is weak, and the magnetic dipole transition becomes relatively stronger and dominating. In $ABaGd_{0\cdot5}(PO_4)_2 : Eu^{3+}_{0\cdot5}$ (where A = Li, Na, and K), emission lines for magnetic ($^5D_0 \rightarrow {}^7F_1$) and forced electric dipole transitions ($^5D_0 \rightarrow {}^7F_2$) were observed (Band *et al* 1999). These are consistent with the earlier reported results (Oomen and van Dongen 1989). The $^5D_0 \rightarrow {}^7F_2$ transition is dependent upon the local symmetry, whereas $^5D_0 \rightarrow {}^7F_1$ emission may be related to local symmetry due to insensitivity to the site symmetry. Since $^5D_0 \rightarrow {}^7F_2$ transition is much stronger than that of the $^5D_0 \rightarrow {}^7F_1$ transition, the Eu^{3+} ion in the calcium silicate prepared by the sol–gel process is situated at the low symmetry sites. The other allowed weak transitions (low intensity) are $^5D_0 \rightarrow {}^7F_0$, $^5D_0 \rightarrow {}^7F_3$, and $^5D_0 \rightarrow {}^7F_4$. Figure 5 (curve b) shows the emission spectrum of doped silicate excited at 267 nm wavelength. Like 399 nm excitation wavelength, prominent peaks are observed at 594 and 618 nm along with a shoulder at 660 nm. The overall emission intensity is drastically reduced. The 267 nm excitation wavelength may correspond to O^{2-} ions. Earlier it has been reported that the charge transfer from ligands (O^{2-} ions) to Eu^{3+} ions would play an important role on the excitation and emission bands of Eu^{3+} ions in fired $MgSiO_3$ gel (Fan *et al* 1996). However, maximum emission output was obtained for 399 nm excitation wavelength in fired $CaSiO_3 : Eu^{3+}$ gel. Therefore, 399 nm wavelength is used for excitation instead of 267 nm. The inset of figure 5 shows the variations of 618 nm peak intensity with the Eu^{3+} concentration in calcium silicate gel for 399 nm excitation wavelength. Experimental photoluminescence intensity was plotted against the concentration. Results show that the Eu^{3+} emission intensity increases in the beginning up to 3 mol% and starts decreasing slowly for higher concentration. This may be due to the concentration quenching of Eu^{3+} emission.

In doped $CaSiO_3$, Eu^{3+} ion enters into Ca^{2+} lattice site. The ionic radii of Eu^{3+} and Ca^{2+} are 0·113 and 0·106 nm, respectively. Since ionic radius of Ca^{2+} is smaller than Eu^{3+}, $CaSiO_3$ host could accommodate only small percentage of impurity ions. Moreover, there is charge imbalance in the host lattice due to doping of trivalent Eu^{3+} cations. In a gel with impurity concentration above 3 mol%, Eu^{3+} ions go to the interstitial sites. This may trap emitted light, resulting into decrease of intensity.

3.4b *PL in (Ca, Ba) $SiO_3 : Eu^{3+}$ and (Ca, Sr) $SiO_3 : Eu^{3+}$*: The excitation spectra of (Ca, Ba) $SiO_3 : Eu^{3+}$ (3 mol%), monitored at 614 nm is shown in figure 6 (curve a). The

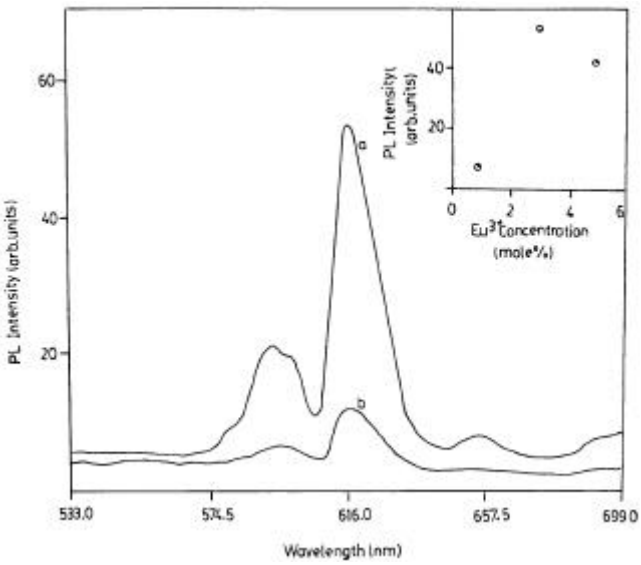

Figure 5. Photoluminescence emission spectrum of $CaSiO_3 : Eu^{3+}$ gel fired at 850°C: a. excited at 399 nm and b. excited at 267 nm wavelength. (Inset shows the variation of emission peak intensity at 618 nm with Eu^{3+} ion concentration).

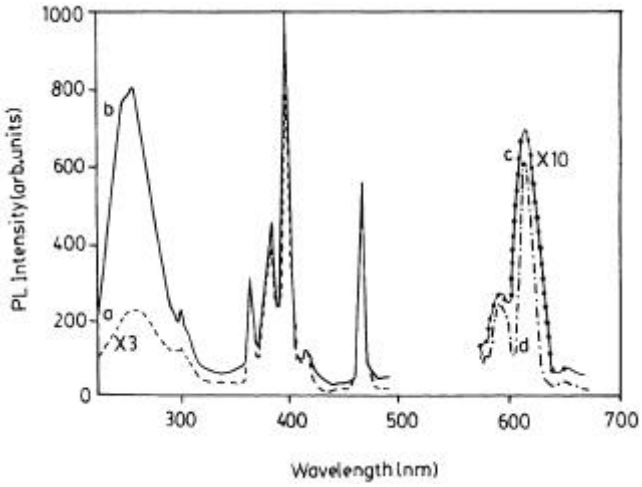

Figure 6. Photoluminescence spectrum of (a) excitation spectrum (l_{em} = 614 nm) of (Ca, Ba) $SiO_3 : Eu$, (b) excitation spectrum (l_{em} = 614 nm) of (Ca, Sr) $SiO_3 : Eu$, (c) emission spectrum (l_{ex} = 254 nm) of (Ca, Ba) $SiO_3 : Eu$ and (d) emission spectrum (l_{ex} = 254 nm) of (Ca, Sr) $SiO_3 : Eu$.

broad band was observed at 254 nm. Besides charge transfer bands are observed at 392 nm. The excitation of Eu^{3+} takes place from the bottom of the $^7F_0$ curve, rising along the straight vertical, until it crosses the charge-transfer state (CTS). Relaxation occurs along the CTS curve. Near the bottom of CTS curve, the excitation is transferred to ^5D_j states. Relaxation to the bottom of the ^5D_j states is followed by light emission downward to ^7F_j states. This model can explain the following experimental findings: (i) No luminescence is found from $^5D_3$ in $Y_2O_2S : Eu^{3+}$, (ii) the luminescence efficiency is higher for phosphors with higher CTS energy (Blasse 1966) and (iii) the quenching temperature of the luminescence from ^5D_j is higher as j (0, 1, 2, 3) decreases. The excited 4*f* states may dissociate into an electron–hole pair.

By taking a model where CTS is a combination of $4f^7$ electron plus a hole, one finds that the resulting spin multiplicities should be 7 and 9. It is the former state that affects optical properties related to the ^7F_j state by spin-restricted covalency. The intensity ratio of the luminescence from $^5D_0 \rightarrow {}^7F_2$ and from $^5D_0 \rightarrow {}^7F_1$ decreases with increasing CTS energy sequentially as $ScVO_4$, YVO_4, $ScPO_4$, and YPO_4, all of which have the same type of zircon structure (Blasse and Bril 1969). The above intensity ratio is small in $YF_3 : Eu^{3+}$ even though Eu^{3+} occupies a site without inversion symmetry (Blasse and Bril 1967). It is to be noted that CTS in fluoride have higher energies than those in oxides. The results suggest that higher CTS energies reduce the strength of the electric dipole transition $^5D_0 \rightarrow {}^7F_2$ in Eu^{3+}. In CTS, electrons in the neighbouring anions are transferred as 4*f* orbitals and results in strong optical absorptions. Optical absorption due to a charge transfer transition are found in Eu^{3+}. CTS absorptions in Eu^{3+} and Yb^{3+} have energies less than 40×10^3 cm^{-1}. They can, therefore, interact with 4*f* levels, leading to $f \rightarrow f$ emissions.

One can conclude that those ions that are easily oxidized to the tetravalent state have lower $4f \rightarrow 5d$ transition energies, while those that are easily reduceable to the divalent state have lower CTS transition energies. It has been confirmed that $4f^0$, $4f^7$ and $4f^{14}$ electron configurations are relatively stable. The optical absorption transition at 254 nm may be related to Eu^{3+}, due to the 4*f* shell. The transition corresponding to wavelength 254 is $^7F_0 \rightarrow {}^5L_6$. The fluorescence lamp is a low pressure mercury discharge lamp with a layer of phosphor particles on the inside surface of a glass tube. The internal radiation which is generated, mostly at 254 nm (85%) is the resonance wavelength of the mercury vapour discharge. The other 15% are distributed among 185, 315, 365, 430, 546 and 578·5 nm. The 254 nm excitation wavelength in (Ca, Ba) $SiO_3 : Eu^{3+}$ and (Ca, Sr) $SiO_3 : Eu^{3+}$ is 100% overlapping to the main mercury discharge wavelength at 254 nm. Therefore, the 254 nm wavelength was selected for the excitation in (Ca, Ba) $SiO_3 : Eu^{3+}$ and (Ca, Sr) $SiO_3 : Eu^{3+}$ instead of 388, 392 and 465 nm. The emission spectra of (Ca, Ba) $SiO_3 : Eu^{3+}$ (3 mol%) is shown in figure 6 (curve c). The strong emission peak observed at the wavelength 614 nm, excited by 254 nm light, corresponding to $^5D_0 \rightarrow {}^7F_2$ transition. Weak peak observed at 594 nm is due to $^5D_0 \rightarrow {}^7F_1$ transition. Strong $^5D_0 \rightarrow {}^7F_2$ transition of Eu^{3+} observed in red region of the spectrum is very important for lamp phosphor application (excitation wavelength is 254 nm).

When the sample is excited by 254 nm light, Eu^{3+} ion is raised to $^5L_6$ from ground state. During emission, Eu^{3+} ion decays stepwise from $^5L_6$ to $^5D_0$ state giving small quanta of energy to the lattice; it decays non-radiatively between $^5L_6$ to $^5D_0$ state. Since the separation between $^5D_0$ and $^7F_2$ is large, the process of step-wise decay stops here and it returns to ground state by giving emission in red and orange (594 nm) regions of the spectrum. In the transition $^5D_0 \rightarrow {}^7F_2$ emission, $J = 2$ and it is an allowed transition. Being the impurity atom, Eu^{3+} does not occupy at the centre of symmetry. It will give both magnetic and electric dipole transition when $J = 1$. However, when $J \leq 6$, where $J = 2, 4, 6$ are allowed transitions, the electric dipole transitions are called forced electric dipole transitions. The transition $^5D_0 \rightarrow {}^7F_1$ gives orange emission. If the Eu^{3+} ions are located at a site i.e. a centre of symmetry in the relevant crystal lattice, only magnetic dipole transitions are possible. The selection rule is $\Delta J = 0, \pm 1$ of Eu^{3+} ions is situated at a centre of symmetry and is brought in $^5D_0$ state, the only possible transition is $^5D_0 \rightarrow {}^7F_1$ corresponding to the wavelength 594 nm. In another sample we have used Sr instead of Ba in several mixed silicate phosphor. In (Ca, Sr) $SiO_3 : Eu^{3+}$ (3 mol%) sample strong excitation peak is observed at 254 nm (l_{em} = 614 nm) due to transition of $^7F_0 \rightarrow {}^5L_6$ (figure 6, curve b). The emission spectra of the sample is shown in figure 6 (curve d). It was observed that the strong emission peak observed at 614 nm (l_{ex} = 254 nm) is due to $^5D_0 \rightarrow {}^7F_2$ transition of red region of the spectrum. In both the phosphors $^5D_0 \rightarrow {}^7F_2$ transitions of Eu^{3+} (at 614 nm) are intensely observed, hence Eu^{3+} ions enter at the centre of symmetry in the crystal lattice.

4. Conclusions

In conclusion, doped $CaSiO_3$ is synthesized by sol–gel process and crystallization temperature appears at about 850–875°C. Small trace of Ca_2SiO_4 is observed in $CaSiO_3$ fired gel. The SEM results show uniform surface morphology of the phosphors and particle sizes are < 3 μm and are very useful in coating purpose. Eu^{3+} emission lines are obtained at 594 and 618 nm. All peaks split due to crystal field and splitting depends upon the firing temperature of the gel.

In (Ca, Ba) $SiO_3 : Eu^{3+}$ and (Ca, Sr) $SiO_3 : Eu^{3+}$, emission are observed at 614 nm when excited by 254 nm. Emission of Eu^{3+} was found to be particularly useful as a red emitting lamp phosphor as it has good sensitivity and

excitation overlapping is quite well with 254 nm of Hg emission. PL intensity of 614 nm peak is 10 times more in (Ca,Ba) $SiO_3 : Eu^{3+}$ phosphor as compared to (Ca, Sr) $SiO_3 : Eu^{3+}$ phosphor. Strong position of Eu^{3+} peak (614 nm) indicates that Eu^{3+} ions are mostly present at the site of centre of symmetry of crystal lattice. Therefore, (Ca, Ba) $SiO_3 : Eu^{3+}$ phosphor may be used as an efficient red lamp phosphor.

References

Ahmadi T S, Haase M and Weller H 2000 *Mater. Res. Bull.* **35** 1869

Avella F J, Sovers O J and Wiggins C S 1967 *J. Electrochem. Soc.* **114** 613

Band A M, Dhoble S J and Pode R B 1999 *Bull. Mater. Sci.* **22** 965

Blasse G 1966 *J. Chem. Phys.* **45** 2356

Blasse G 1970 *J. Lumin.* **1**, **2** 766

Blasse G and Bril A 1967 *Philips Res. Rep.* **22** 481

Blasse G and Bril A 1969 *J. Chem. Phys.* **50** 2974

Blasse G and Bril A 1970 *Philips Tech. Rev.* **31** 304

Cavouras D, Kandarakis I, Nomicos C D, Panayiotakis G S and Fezoulidis J 2000 *Appl. Radiat. Isot.* **32** 119

Cich M, Kim K, Choi H and Hwang T 1998 *Appl. Phys. Lett.* **73** 2116

Crawford M K and Bixner L H 1991 *J. Lumin.* **48 & 49** 37

Fan X, Wang M, Yu Yiu and Wu Q 1996 *J. Phys. Chem. Solids* **57** 1259

Gomes De Mesquita A H and Bril A 1969a *J. Electrochem. Soc.* **116** 871

Gomes De Mesquita A H and Bril A 1969b *Mater. Res. Bull.* **4** 643

Haft H H and Thornton W A 1972 JIES

Jain S, Gending J and Yuanfu H 1992 *J. Mater. Sci. Lett.* **11** 409

JCPDS (Joint Committee on Powder Diffraction Standards), Amer. Soc. for Testing Materials (PA) Card Number 27-88

Kandarakis I, Cavoures D, Prassopoulos P, Kanellopoulas E, Nomicos C D and Panayiotakis G S 1998 *Appl. Phys.* **A67** 521

Koedam M and Opstelten J J 1971 *Light Res. Tech.* **3** 205

Kurczyk H G and Wuhrer J 1971 *Interceram.* **2** 119

Lenggoro I W, Iskandar F, Mizushima H, Xia B, Okuyama K and Kijima N 2000 *Jpn. J. Appl. Phys. Lett.* **39** L1051

Leskela M and Niinitso L 1992 *Mater. Chem. Phys.* **31** 7

Lin J, Sanger D U, Mennig M and Barner K 2000 *Thin Solid Films* **360** 39

Lu S W, Copeland T, Lee B I, Tong W, Wasgner B K, Park W and Zhang F 200l *J. Phys. Chem. Solids* **62** 777

Meijerink A and Blasse G 1989 *J. Lumin.* **43** 283

Moharil S V 1994 *Bull. Mater. Sci.* **17** 25

Ohnishi H 1983 *Ann. Rev. Mater. Sci.* **19** 83

Oomen E W J L and van Dongen A M A 1989 *J. Non-Cryst. Solids* **111** 205

Otvos N and Peto A 1998 *Rad. Measur.* **29** 319

Ouyang X, Kital A H and Xiao T 1996 *J. Appl. Phys.* **79** 3229

Peters T E 1969 *J. Electrochem. Soc.* **116** 985

Pode R B and Dhoble S J 1997 *Phys. Status Solidi(b)* **203** 571

Rabinovich E M, Shmulovich J, Fratello V J and Kopylov N J 1987 *Am. Ceram. Soc. Bull.* **66** 1505

Raue R, Vink A T and Welker T 1984 *Philos. Tech. Rev.* **44** 335

Smets B M J 1987 *Mater. Chem. Phys.* **16** 283

Sohn K S, Cho B, Chang H, Park H D, Choi Y G and Kim K H 2000 *J. Eur. Ceram. Soc.* **20** 1043

Su K, Tilley D T and Sailor M J 1996 *J. Am. Ceram. Soc.* **118** 3459

Upadeo S V and Moharil S V 1996 *Rad. Eff. Def. Solids* **138** 167

Wanmaker W L and ter Vrugt J W 1967 *Philips. Res. Rep.* **22** 355

Wanmaker W L, Bril A, ter Vrugt J W and Broos J 1966 *Philips Res. Rep.* **21** 270

Welker T 1991 *J. Lumin.* **48 & 49** 49

Zhang H X *et al* 2001 *Mater. Chem. Phys.* **68** 31